Coupling Effect of State-of-Charge and Strain Rate on the Mechanical Behavior of Electrodes of 21700 Lithium-ion Battery

Aditya Sonwane[1,2], Chunhao Yuan[1, 2], Jun Xu[1, 2]

[1]*Department of Mechanical Engineering and Engineering Science, The University of North Carolina at Charlotte, Charlotte, NC 28223, USA.*

[2]*Vehicle Energy & Safety Laboratory (VESL), North Carolina Motorsports and Automotive Research Center, The University of North Carolina at Charlotte, Charlotte, NC 28223, USA.*

Abstract

As an emerging type of high-density lithium-ion batteries for electric vehicles, 21700 cylindrical batteries may suffer inevitable mechanical vibrations, curbstone impact/penetration and crash accidents, which probably induce internal short circuit, thermal runaway, and more catastrophic events such as fire/explosion. Therefore, exploring the mechanical behavior quantitively serves as a cornerstone for a better understanding of the safety behaviors of batteries. This paper focuses on the characterization of the tensile mechanical behavior of the electrodes under different SOCs coupled with strain rate effect. In the meantime, a numerical computation model is also established to provide a fundamental understanding of the electrode deformation. We discover that both anodes and cathodes are highly anisotropic at various electrochemical statuses, and strong strain rate dependency can be observed. Results provide

an in-depth and systematic characterization of the mechanical behaviors of the electrodes and a powerful tool for the future design, evaluation, and manufacturing of safer batteries.

1. Introduction

Lithium-ion batteries (LIBs) have been widely used as the power source of electric vehicles[1-6] due to their high energy and power densities [5-8]. Also, LIBs have gained increasing popularity due to the soaring demand for the mobility of devices such as cell-phones, computers, communication devices, and among others [7, 9-12]. In addition, an ever-increasing number of catastrophic accidents were reported, where the internal short circuit, thermal runaway or even fire/explosion under abusive mechanical loading[1, 7, 8, 12-14]. Such engineering application scenarios ask for a comprehensive understanding of the mechanical and electrochemical behaviors of the cell as well as the battery component materials.

Electrodes are key components containing active particles, binder, and the substrate foils. The mechanical loading and abusive tests were conducted on the electrode level individually, considering the crack propagations [15] and the battery cells all together [12, 13, 16, 17] in 18650 cylindrical batteries, various sizes of pouch cells, and prismatic cells. The mechanical loading is the primary source that causes the deformation, structural failure, and material fracture in the battery where the electrochemistry performance will be greatly reduced [6]. Macro-scale studies have thoroughly provided with an idea about the mechanical behavior of the battery [16], and the micro-scale studies have aided the understanding of stress evolution, stress distribution following the mechanical abuse over the battery electrodes, seperators and even the current collectors [5]. Alongside these abusive tests which related to battery safety, the SOC (State-of-Charge) dependency and strain rate studies coupling them together has revealed the understanding of the ISC (Internal Short Circuit) [5, 6, 16, 18]. The new mechanical model for computation is established by considering the dynamic loading and SOC effects [16]. Study on the SOC-dependent mechanical integrity behavior is crucial for understanding the crashworthiness of LIBs, especially in the situations like, when the battery charges and discharges, leading to the change in SOC value [19] and the multiphysical behavior

4 of cylindrical LIB from cell deformation to short-circuit is described by the modeling framework [13]. Xu et al. [19] performed a series of mechanical tests for two types of separators, considering both the anisotropy and environment solvent effects coupled with the strain rate effect [3, 6, 12].

Recently, more focus has been cast on the mechanical behaviors of the battery materials with the consideration of the electrochemical status, such as to understand the real-world scenarios. For example, Xu et al. [20] study of SOC and its dependency due to structural response of the cell which is a crucial topic considering the crash safety and ISC in the batteries [8, 14]. Mechanical loading experiments validating the numerical simulations of LIB cells under dynamic loading have laid a foundation for research on LIB safety design [16]. Experiments and mechanical constitutive models for sandwiched anode and cathode developed can help facilitate a quantitative prediction of the mechanical responses and capture the stress state of inner components of LIB [5]. Study of the location of failure of the electrode, crack orientation and length, area of the fractured region [15], leading to ISC and then to thermal runaway through FEM (Finite Element Modeling) and experiments of mechnical penetration over cylindrical, pouch cells provide a safety design of LIBs [1, 12, 21].

The SOC dependent mechanical behavior of the cell stems from the SOC dependent properties of the component materials, and naturally, the anodes and cathodes play the dominant role [20]. Intuitively, such SOC dependency will become more evident in the cases of high energy density batteries. To bridge this gap, aiming at the new generation of cylindrical batteries for electric vehicles, we perform comprehensive characterizations on the mechanical behaviors of the cathodes and anodes upon various strain rates in mechanical abusive loading. In the meantime, the various SOC statuses are also considered. Numerical simulation models are established to assist the in-depth understanding of the mechanical deformation and failure mechanisms.

2. Methodology

2.1 Experimental

NCA (Nickel Cobalt Aluminium Oxide) cathode and graphite anode cells were chosen for the study. The 21700 M50 battery cell here has a capacity of 5000mAh with a maximum 4.2 V as the charge voltage and 2.5 V as the minimum cut off voltage. The electrode samples for the experiment, i.e., cathode and anode (with active particles, binders, and foils), were extracted from the battery in different SOCs, with careful removal of the outer coverings and the shell of the battery. The jellyroll consists of multiple layers in following order anode, separator, cathode, separator [5] rolled in a manner to fit inside the stainless-steel casing. Electrodes are a three-layered structure stacked as the current collector sandwiched between the layer of active material [6]. Both the cathode and anode current collector materials (aluminum and copper, respectively) are coated with active particles. The thickness of each sample is discussed further in this study. Working on higher SOC is hazardous and of high-risk. The study of the electrodes even at lower SOC has proven to provide sufficient data to obtain the SOC behavior. Hence, SOC=0, 0.2, 0.4, and 0.6 were selected to investigate the SOC effect on the mechanical behavior of electrodes. 1 C rate was adopted to charge for different SOCs. All cells used in experiments here are fresh with same charging rate.

Fig. 1 shows the process of how the battery was cut to take out the electrodes for further processes. The electrodes, after removal from the shell, were sampled or cut into samples for testing with accurate measurements for each sample in three orientations for the electrode roll. 0°, 45°, and 90° were the orientations selected to study the anisotropic behavior of the electrodes (Fig. 2). The process of sampling from the jellyroll to the individual samples is shown in Fig. 2.

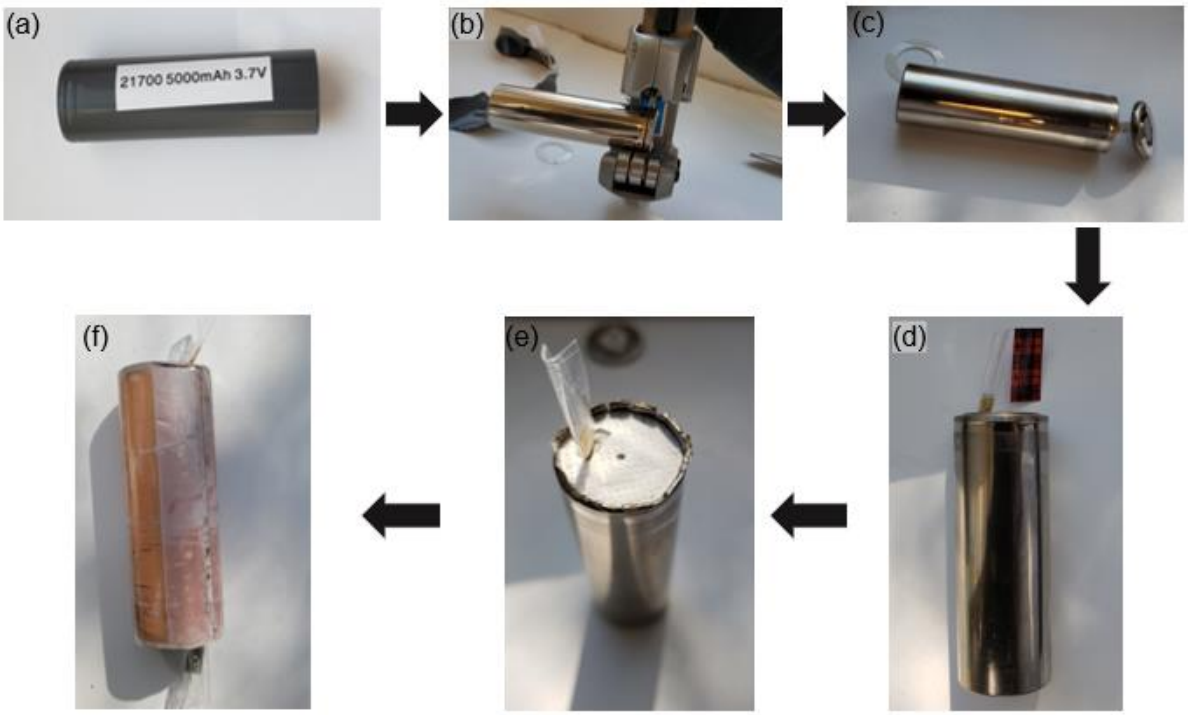

Fig.1. Illustration of battery cutting stages: (a) Battery sample with different SOCs (i.e. 0, 0.2, 0.4 and 0.6)out removed from cycler with 1C charging rate, (b) The battery mounted on the tool to cut off the battery cap, (c) The battery with the cap removed, (d) Anode covered with tape to avoid internal short circuit by accidental touching with cathode, (e) Shell cutting to remove the jellyroll, (f) Jellyroll after removing the shell.

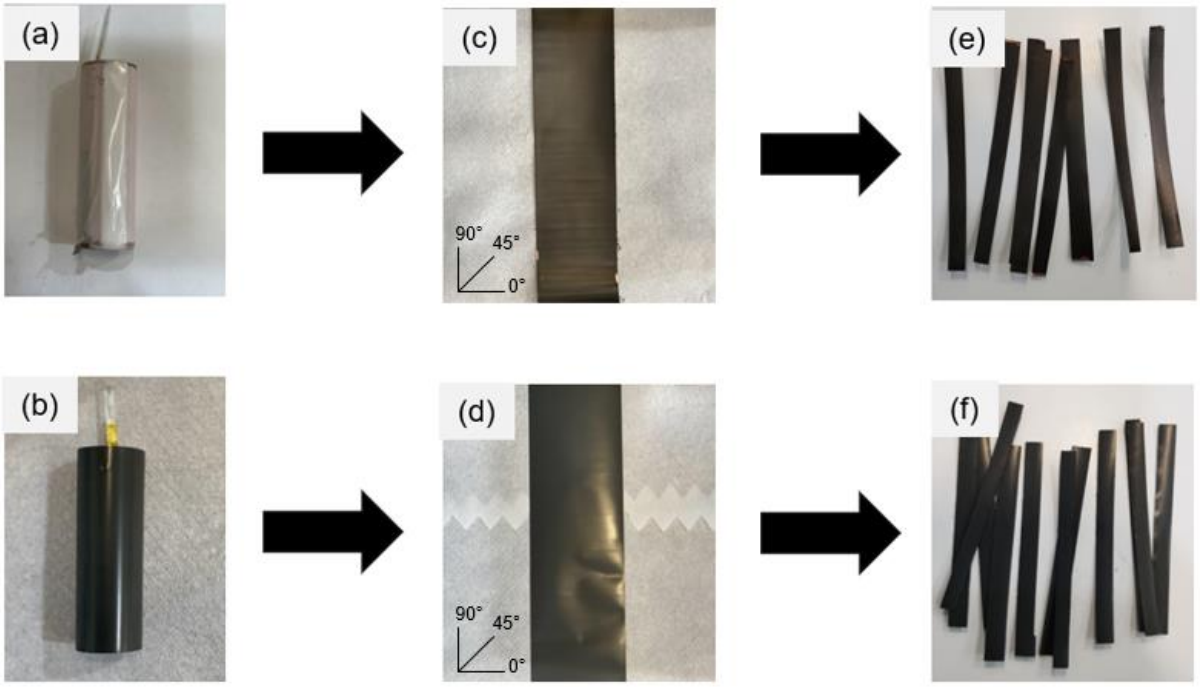

Fig.2. From electrode rolls to testing samples (a) Anode Electrode roll separated from the jellyroll, (b) Cathode Electrode roll after separation from jellyroll and removal of separator, (c) Anode electrode flattened on the desk showing the orientation 0°, 45°and 90° in which the electrode will be sampled,

(d) Cathode electrode flattened on the desk showing the orientation 0°, 45°and 90° in which the electrode will be sampled, (e) Anode samples cut out from the roll at 0°, (f) Cathode sample cut out from the roll at 0°.

Tensile experiments for all samples were performed on the Instron E3000 machine with maximum dynamic loading of 3 kN, static loading of 2.1 kN, and ±0.5% indicated load accuracy. Four strain rates were considered for the tensile experiments of the samples that are $0.01s^{-1}$, $0.1\ s^{-1}$, $1\ s^{-1}$, and $10\ s^{-1}$. Each loading scenario had a minimum of 3 repeated tests to ensure the reliability of the data. To prepare the current collector samples ready for the experiment, we cleaned the electrode with 70% ethyl alcohol with delicacy without producing any damage to the current collector foil.

Referring to the work on the tensile experiment carried out by Yuan et al. [22] and Lai et al. [23], the following process was carried out prior to testing. Each sample tested had its length, width, and thickness measured before the tensile test. The length *L* of samples ranged from 40 mm to 60 mm, and the width for the samples ranged from 4 mm to 6.2 mm. The anode with active materials had the thickness measured as 0.198±0.002 mm , 0.203±0.006 mm , 0.205±0.004 mm and 0.211±0.006 mm for SOC=0, 0.2, 0.4, and 0.6, respectively. For cathode, the thickness was 0.167±0.003 mm, 0.173±0.004 mm, 0.171±0.005, and 0.167±0.002 mm for SOC=0, 0.2, 0.4, and 0.6, respectively. . The thicknesses of the the current collectors of the anode and cathode were measured as 0.017±0.003 mm and 0.027±0.003 mm, respectively. There was not much change in the thickness of the current collectors with increasing SOC since the lithiation/delithiation occurs only within the active material region, and the current collectors are free of volume change. During charging and discharging, the lithium ions move between cathode and anode, which involves a series of chemical reactions accompanied by the mass transfer process. The chemical compositions of the active material of the cathode and the graphite coating of anode vary due to lithium-ion intercalation and deintercalation. This can

affect the mechanical properties of active particles, which may further influence the overall mechanical performance of the battery cell [7]. Battery charging will also lead to volume expansion in a limited repressed space, which causes internal stress hence determining the mechanical and electrical behaviors of the cell [5, 9, 10].

Each sample was clamped with caution during the experiment in the Instron E3000 machine, as shown in Fig. 3(a). Each strain rate had a different test setup drafted and simulated as needed with different velocities as 0.4 mm/s, 4 mm/s, 40 mm/s and 400 mm/s for $0.01s^{-1}$, $0.1\ s^{-1}$, $1\ s^{-1}$ and $10\ s^{-1}$ strain rates, respectively. Depending on the strain rates, velocity was calculated and fed to the machine to proceed with the tensile testing. The electrode samples with active materials and the current collectors for SOC=0 after the tensile test are shown in Figs. 3 (b)-(e).

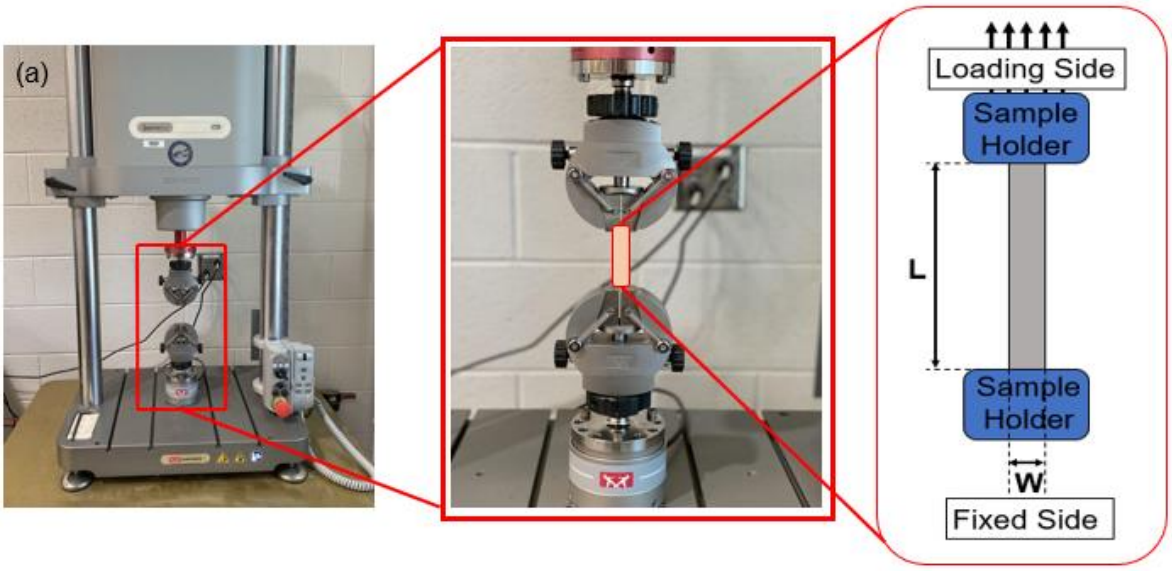

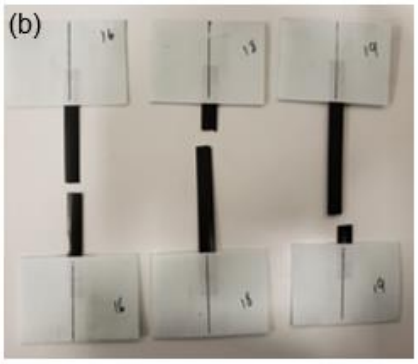

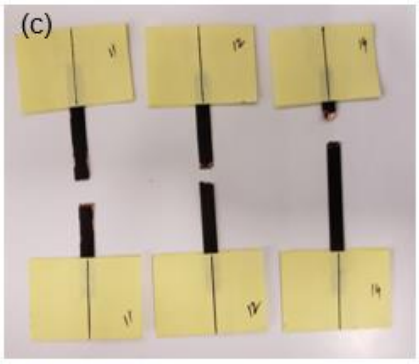

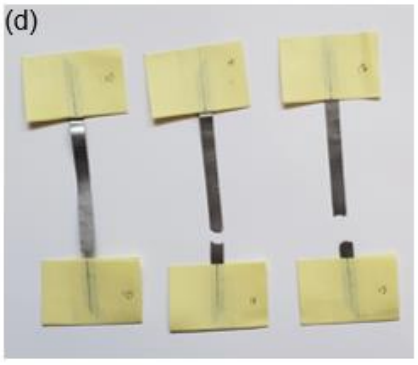

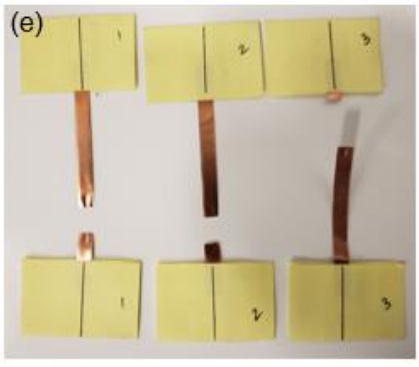

Fig.3. (a) Illustration of the tensile testing experiment setup on Instron 3000 loading machine, Samples showing fracture after tensile test: (b) cathode electrode with active material for SOC=0 and orientation=0°, (c) anode electrode with active material for SOC=0 and orientation=0°, (d) cathode current collector for SOC=0 and orientation=0°, (e) anode current collector for SOC=0 and orientation=0°.

2.2 Numerical simulation

To further investigate the mechanical behavior of the battery electrodes, numerical simulation was carried out based on the ABAQUS platform. Each electrode has different material properties, which were calculated from the experiment data. The density change can be observed in the electrodes more notably in the anode. Since the change in the density with an increase in SOC is below 7 % it is not consequential to use these distinct values for the simulation purpose. A value compatible with all the samples for different SOC was selected from the literature [14, 24] to be used for numerical simulations in the study. The density ρ of the electrodes was taken from the literature [14, 24] while other mechanical properties such as the yield stress σ_y, yield strain ε_y, failure stress σ_f, failure strain ε_f along with elastic modulus E were calculated from the stress-strain curves of the electrodes from the tensile test, as shown in Fig. 4 (a). The modulus E calculated for the current collectors, i.e., for the aluminum and copper thin films, will be smaller than that of the modulus values of these materials in mass. The modulus of electrolytic copper foils is 70 GPa, and that of rolled copper foils is around 50 GPa which was smaller than the modulus of bulk copper i.e., 120 GPa and similar variation in the parameters is observed in the our previous studies [25, 26] that is the calculated modulus for anode current collectors is 29.3 GPa the calculated values vary for various battery sample and type. Table 1 shows the details of density ρ and modulus E for each electrode sample.

Johnson-Cook model is considered here to describe the strain rate dependent mechanical behaviors [1, 3] (Eq. (1)). Based on the experimental data, a curve fitting code was used to get the plasticity stage parameters using the MATLAB platform to establish the constitutive models. The plasticity stage is then described in the simulation based on the stress-strain curves. Ductile damage is used to govern the failure with triaxiality as 0.33 and the failure

displacement as 0.003 mm with changing strain rate and failure strain ε_f in each simulation. All details regarding the Johnson-Cook model are given in Refs. [8, 16]:

$$\sigma = [A + B*(\varepsilon_{pl})^n][1 + C*\ln(\varepsilon_{pl} / \varepsilon_0)] \quad \text{Eq. (1)}$$

where σ is plastic stress, ε_{pl} is the plastic strain, ε_0 is reference strain, A, B, C, and n are material parameters. The ratio ($\varepsilon_{pl}/ \varepsilon_0$) is a dimensionless parameter where the plastic strain is changed as needed. The reference strain used in the simulation and MATLAB code is 0.01 s^{-1}.

For the meshing of the electrode designed as model 1 mm mesh size was selected with C3D8R as the element type. For boundary condition setups, similar to the experimental setup, one side of the sample is clamped, and all the other sides are only free for the displacement along the sample length direction. The Johnson-cook model is chosen in ABAQUS, and parameters are input from the above fitting process. The loading condition is given via the displacement of the free end of the sample. Abaqus dynamic/explicit algorithm was used. Note that the minimum kinetic energy is maintained such that the quasi-static loading is ensured. The total time input for the simulation in step is 0.01 s. A detailed illustration of the model settings is represented in Fig. 4 (b).

Table.1. Material properties: Young's modulus E and density ρ of the samples for different material orientations.

Sample	SOC	0°		45°		90°	
		Modulus (E) (MPa)	Density(ρ) (kg/m^3)	Modulus (E) (MPa)	Density(ρ) (kg/m^3)	Modulus (E) (MPa)	Density(ρ) (kg/m^3)
Cathode with active material	0	4819.423	2890	3003.39	2890	3994.851	2890
Anode with active material	0	3327.66	1640	3719.46	1640	2718.84	1640
Cathode current collector	0	31364.877	2700	27999.005	2700	26408.218	2700
Anode current collector	0	20406.536	8930	29282.305	8930	30912	8930
Anode with active material	0.2	--	--	3339.13	1640	--	--
Anode with active material	0.4	--	--	6673.575	1640	--	--
Anode with active material	0.6	--	--	9826.086	1640	--	--

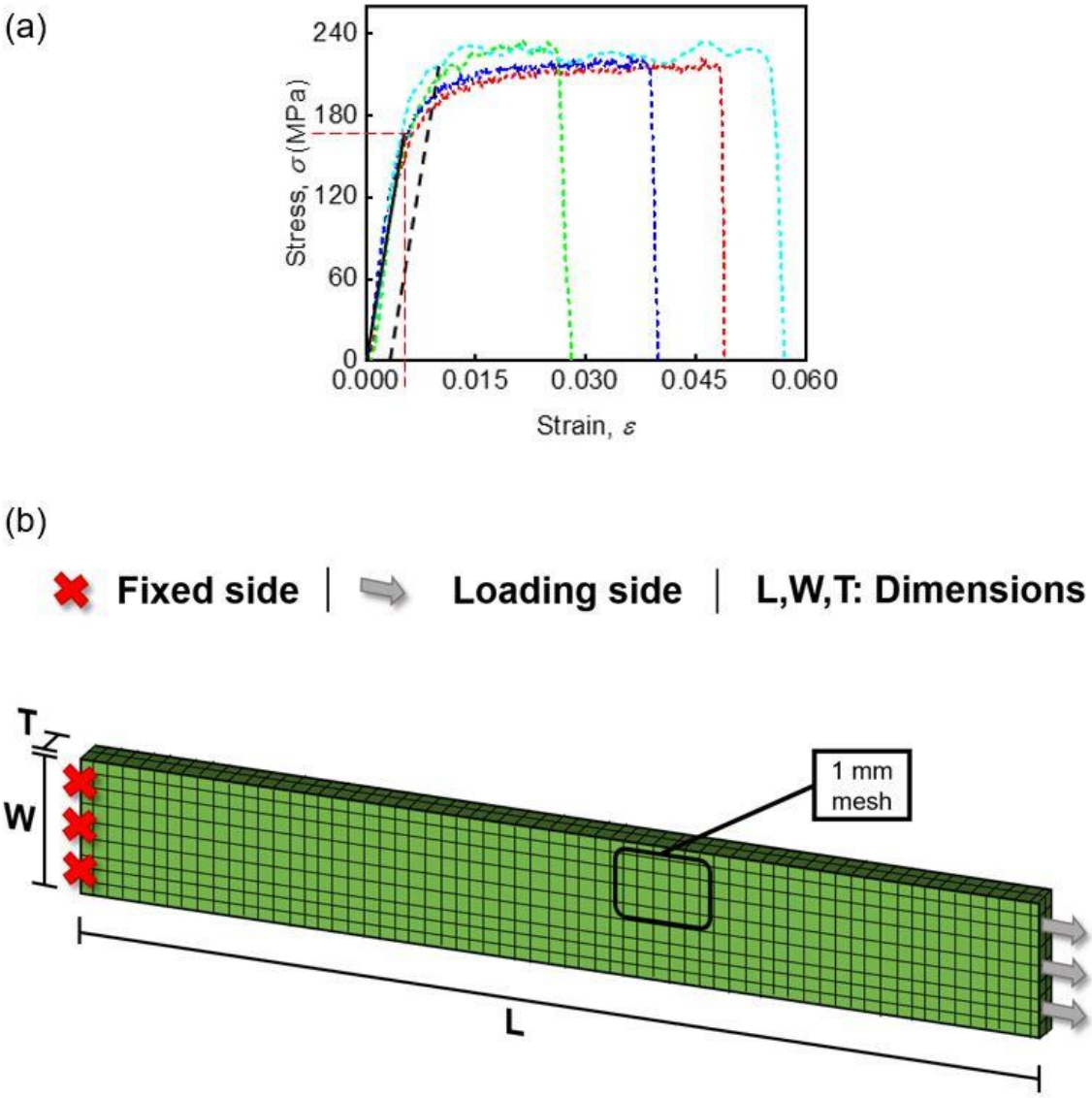

Fig.4. Illustration of: (a) Young's modulus E and yield calculation from stress-strain curves of anode current collector samples at SOC=0 and orientation=45°, (b) boundary conditions applied to the sample used in numerical simulation with mesh and dimension.

3. Results

3.1 Typical experiment results

The stress-strain curves of each electrode with SOC=0 for the same angle orientation i.e., 45° in this case for different strain rates, are shown in Fig. 5. As can be seen from Fig. 5, all curves firstly show the linear elastic stage, followed by the yielding point and the plastic

stage. For cathode, anode, current collectors, the stress in the plastic stage still increases until the failure points, indicating an obvious strain hardening effect.

All the electrodes have shown the common tendency that as the strain rate increases, the stress of the sample as well increases, showing an obvious strain rate effect. The failure strain ε_f is nearly the same, although not identical. Except for anode and cathode with the active material, a considerably differentiating failure strains ε_f can be seen for each strain rate sample for both current collectors. For anode and anode current collector, the failure strain ε_f shows a decreasing trend with increasing strain rates, as is shown in Figs. 5 (b) and (d).

The SOC effect can be seen for electrodes with active materials. A change that can be observed is that the thickness was increased for both anode and cathode. The increase in SOC makes the stress of the electrode for anode with active material rise as well, which can be clearly be seen from Fig. 6. As the anode active material is brittle in nature when taken out from the battery, it became even more fragile as the battery with higher SOC, which is an opposite case in the cathode electrode active material. Here the active material gets a stronger bond to the current collector for higher SOC compared to SOC=0. To understand the material properties, we take further discussion on the modulus E of the electrodes with different SOC in the Discussion part. As Table 1 shows, the anode gets higher elastic modulus E for higher SOC making it more prone to exhibit higher stress-strain curves during the tensile tests.

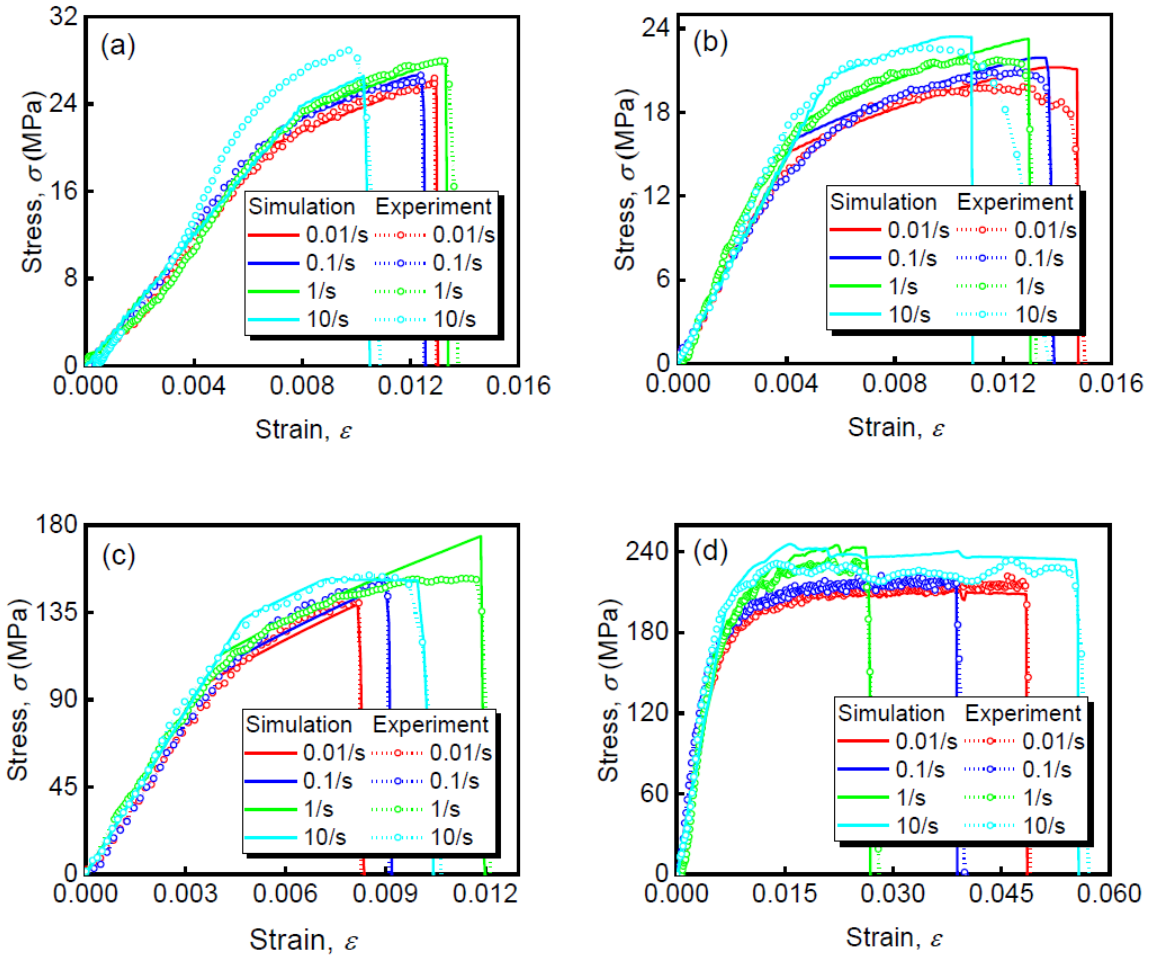

Fig.5. Stress vs strain comparison of experiment and simulation curves at 0.01/s, 0.1/s, 1/s, 10/s strain rates along 45° for: (a) cathode electrode with active material at SOC=0, (b) anode electrode with active material at SOC=0, (c) cathode current collector at SOC=0, (d) anode current collector at SOC=0.

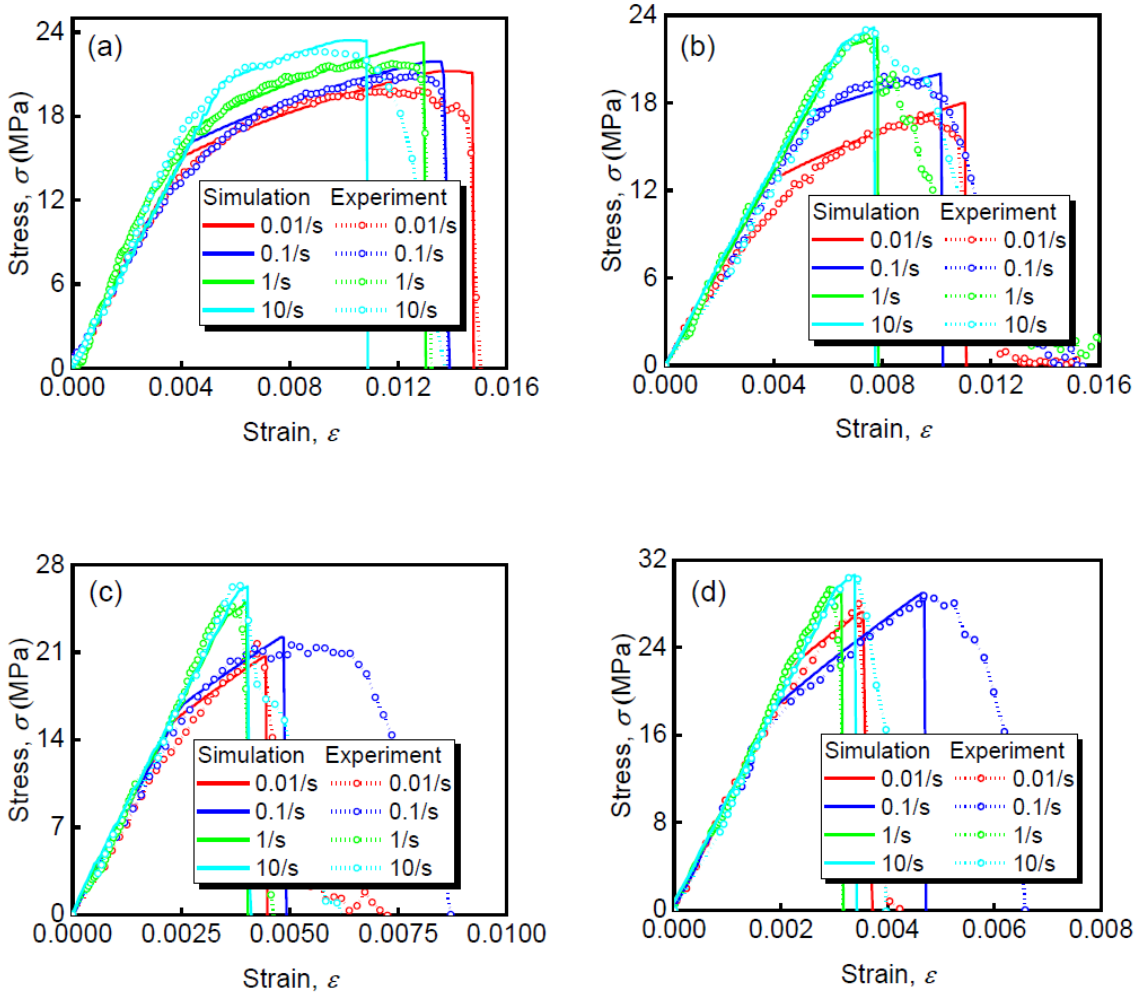

Fig.6. Stress vs strain comparison with different strain rates for anode electrode with active material samples for different SOC along 45° with simulation results: (a) SOC=0, (b) SOC=0.2, (c) SOC=0.4, (d) SOC=0.6.

3.2 Numerical simulation validation.

Since anode is highly dependent on the SOC, the experiment findings validated the simulations for anode with active material for all the mentioned strain rates and state of charges. The simulation results and their comparisons with the experimental curves are given in Fig. 6. From simulation curves, we can see the failure strain ε_f reduces as the strain rate increases as simulation pick up on the failure easily. As Figs. 5 and 6 shown, the simulation can not only describe the elastic stage but also can predict the yielding and plastic stage well for different strain rates and SOCs. Thus, a good description of the mechanical behaviors validates the numerical computational model. Fig. 7 shows the contour plots for anode current collector for

each strain rate (i.e., 0.01 s^{-1}, 0.1 s^{-1}, 1 s^{-1}, and 10 s^{-1}). These plots show the Von Mises stress at different stages of the stress-strain curve showing how the sample experiences the stress throughout loading. These contours are from the start of the plastic stage until the failure of the sample. It is observed that the initial stress experienced by the sample at the start of the plastic stage increments as the strain rate increments from 0.01 s^{-1} to 10 s^{-1}. The higher initial stress leads to higher plastic stress after the yielding. The stress in Point 4 shows the maximum stress of the sample at fracture as well as the fracture point at that maximum stress point over the sample in Figure 7. This fracture point is just about close to the fracture point from experimental samples; hence, validating the simulation.

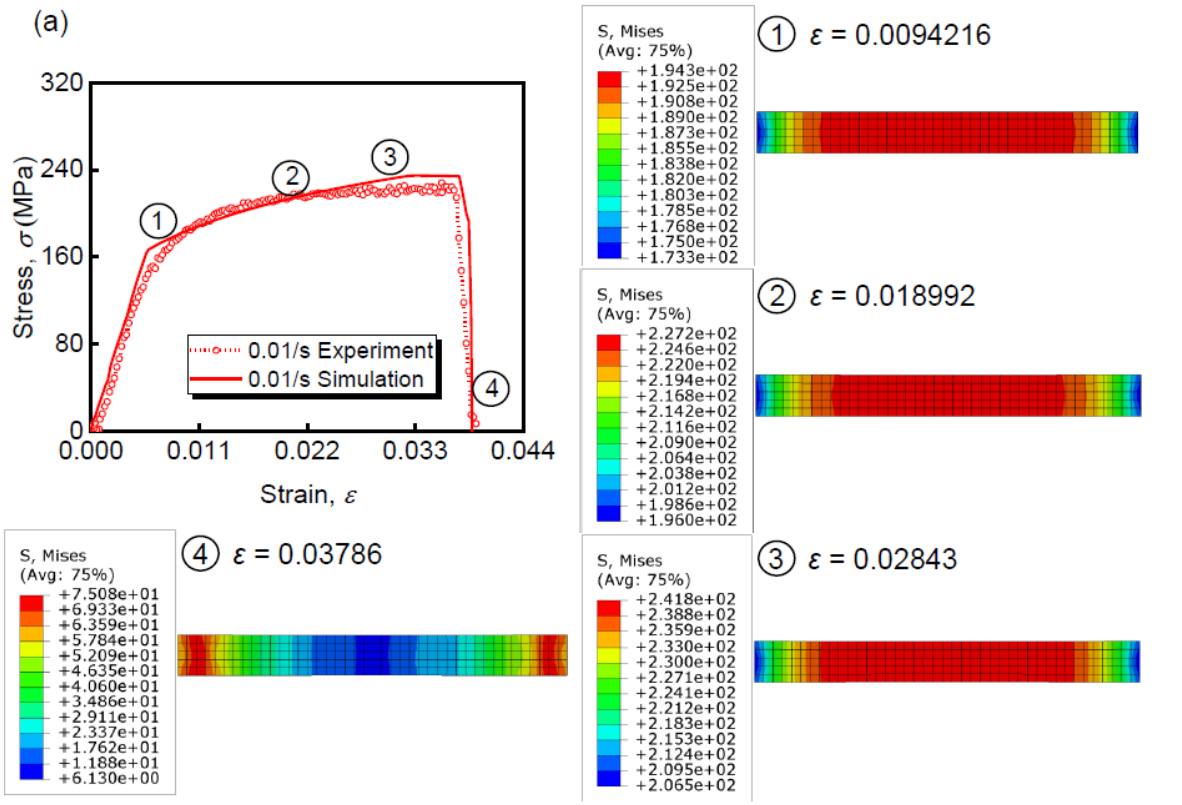
(a)
Stress, σ (MPa)
320
240
160
80
0
0.000
0.011
0.022
0.033
0.044
Strain, ε
0.01/s Experiment
0.01/s Simulation
1
2
3
4
S, Mises
(Avg: 75%)
+1.943e+02
+1.925e+02
+1.908e+02
+1.890e+02
+1.873e+02
+1.855e+02
+1.838e+02
+1.820e+02
+1.803e+02
+1.785e+02
+1.768e+02
+1.750e+02
+1.733e+02
① ε = 0.0094216
+2.272e+02
+2.246e+02
+2.220e+02
+2.194e+02
+2.168e+02
+2.142e+02
+2.116e+02
+2.090e+02
+2.064e+02
+2.038e+02
+2.012e+02
+1.986e+02
+1.960e+02
② ε = 0.018992
+2.418e+02
+2.388e+02
+2.359e+02
+2.330e+02
+2.300e+02
+2.271e+02
+2.241e+02
+2.212e+02
+2.183e+02
+2.153e+02
+2.124e+02
+2.095e+02
+2.065e+02
③ ε = 0.02843
+7.508e+01
+6.933e+01
+6.359e+01
+5.784e+01
+5.209e+01
+4.635e+01
+4.060e+01
+3.486e+01
+2.911e+01
+2.337e+01
+1.762e+01
+1.188e+01
+6.130e+00
④ ε = 0.03786

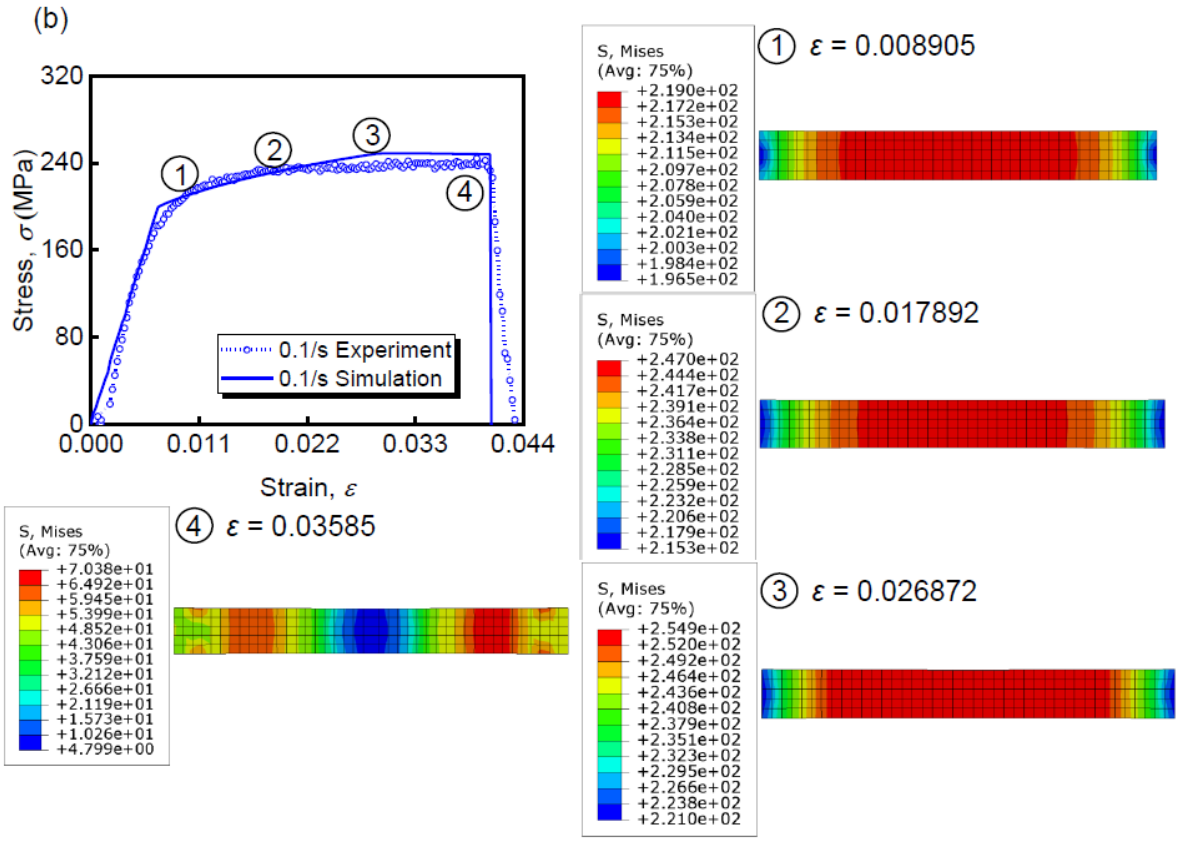
(b)
Stress, σ (MPa)
320
240
160
80
0
0.000
0.011
0.022
0.033
0.044
Strain, ε
0.1/s Experiment
0.1/s Simulation
1
2
3
4
S, Mises
(Avg: 75%)
+2.190e+02
+2.172e+02
+2.153e+02
+2.134e+02
+2.115e+02
+2.097e+02
+2.078e+02
+2.059e+02
+2.040e+02
+2.021e+02
+2.003e+02
+1.984e+02
+1.965e+02
① ε = 0.008905
+2.470e+02
+2.444e+02
+2.417e+02
+2.391e+02
+2.364e+02
+2.338e+02
+2.311e+02
+2.285e+02
+2.259e+02
+2.232e+02
+2.206e+02
+2.179e+02
+2.153e+02
② ε = 0.017892
+2.549e+02
+2.520e+02
+2.492e+02
+2.464e+02
+2.436e+02
+2.408e+02
+2.379e+02
+2.351e+02
+2.323e+02
+2.295e+02
+2.266e+02
+2.238e+02
+2.210e+02
③ ε = 0.026872
+7.038e+01
+6.492e+01
+5.945e+01
+5.399e+01
+4.852e+01
+4.306e+01
+3.759e+01
+3.212e+01
+2.666e+01
+2.119e+01
+1.573e+01
+1.026e+01
+4.799e+00
④ ε = 0.03585

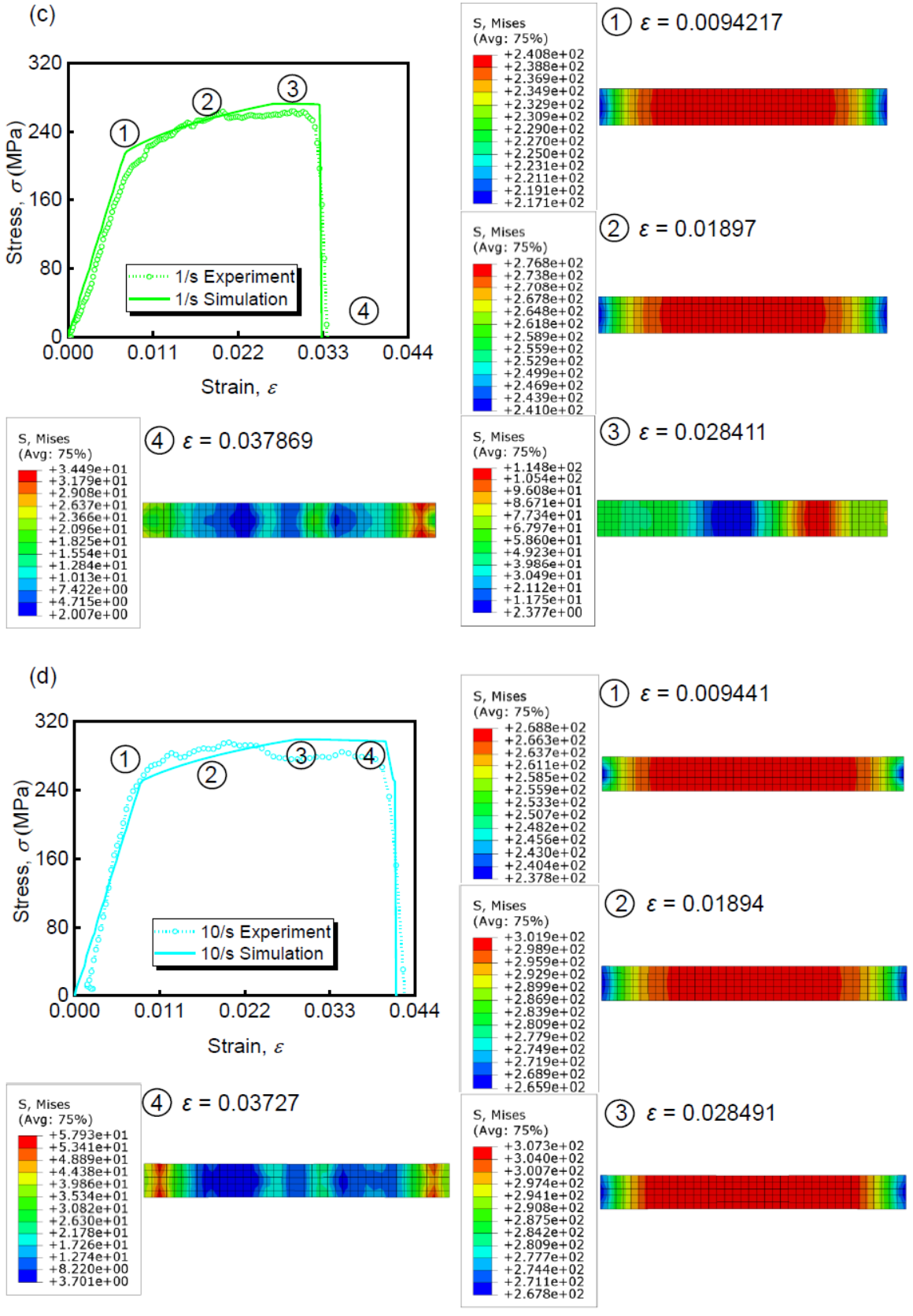

Fig.7. Stress vs strain comparison of anode current collector with simulation results showing contour plots at various instances from start of plastic stage to failure at SOC=0 along 0° for the following strain rates: (a) 0.01/s, (b) 0.1/s, (c) 1/s, (d) 10/s.

4. Discussion

4.1 Anisotropy effect

As mentioned in the experiment part, 0°, 45° and 90° for each electrode and the corresponding current collectors as well were selected for the experiment to study the anisotropy effect, with all the strain rates (i.e., 0.01 s^{-1}, 0.1 s^{-1}, 1 $s^{-1,}$ and 10 s^{-1}) for the SOC=0. The 0° sample orientation is the machine direction, 90° sample orientation is the rolling direction of the electrodes and separators. 45° angle orientation is exactly midway between the 0° and 90° samples. These orientations of the electrodes are represented in Figs. 2 (c) and (d) for anode and cathode, respectively.

Each of the electrodes and the current collectors follows the consistent trend with SOC, i.e., the stress-strain curve lifts as the SOC increases. The modulus E for cathode, anode and current collectors for each strain rate were calculated, which showed minor variations among strain rates. As the elastic stage for each sample mention for each strain rate has the same for experimental curves (which can be noted from the comparison curves of Figs. 5, 8, and 9) a common value was chosen mentioned in Table 1. The experiments conducted here for all the material orientations with all the strain rates for SOC=0 provide validation for simulation similar to discussed earlier in this study.

Observing the curves for all the material orientations in Figs. 8 and 9, we can infer that the 0° samples are stronger than 45° and 90° samples for the cathode, anode current collector (copper foil), and cathode current collector (aluminum foil). However, in the case of the anode electrode in 45° sample is dominating as they have the highest stress. Table 1 shows Young's modulus E for each orientation, cathode electrode 0° has the largest modulus E=4819.42 MPa, the 45° sample has the smallest E=3003.39 MPa, and the 90° sample in between them with E=3994.85 MPa. It can be deduced that since the 0° angle sample does not experience

much loading when they are rolled into the jellyroll due to the higher Young's modulus E. In contrast, 90° samples are under rolling, which makes them stronger than 45° samples as these samples are semi-rolled, making them less flexible. Since the current collector for the cathode is just an aluminum foil, it shows that the 0° samples have the largest elastic modulus E =31364.87 MPa, 90° samples have the smallest modulus E =26408.21 MPa in the cathode current collector, and 45° sample having modulus E =27999 MPa in between 0° and 90° samples. As for the anode electrode sample, the 45° samples have the largest modulus E =3719.46 MPa followed by a 0° sample with E =3327.66 MPa and then lowest for 90° with E =2718.84 MPa. After the anode electrode is flattened out on the table during sampling, the active material, and current collector are strongly bonded in at 45° orientation. In the 0° sample, it is strong as well, but due to rolling, the active material losses little flexibility when flattened, similarly for 90° samples, the active material actually is most brittle than the other two orientations. This gives us an idea about the variation occurring in the modulus E at different orientations. For anode current collector being just a copper foil, the modulus E =30912 MPa is largest at 90° followed by 45° with E =29282.3 MPa and smallest for 0° i.e. E =20406.53 MPa exactly opposite to cathode current collectors. This shows anisotropicity through the current collector. The yield stress σ_y varies as well with the orientation and is more dependent on strain rates, which will be discussed in the next section.

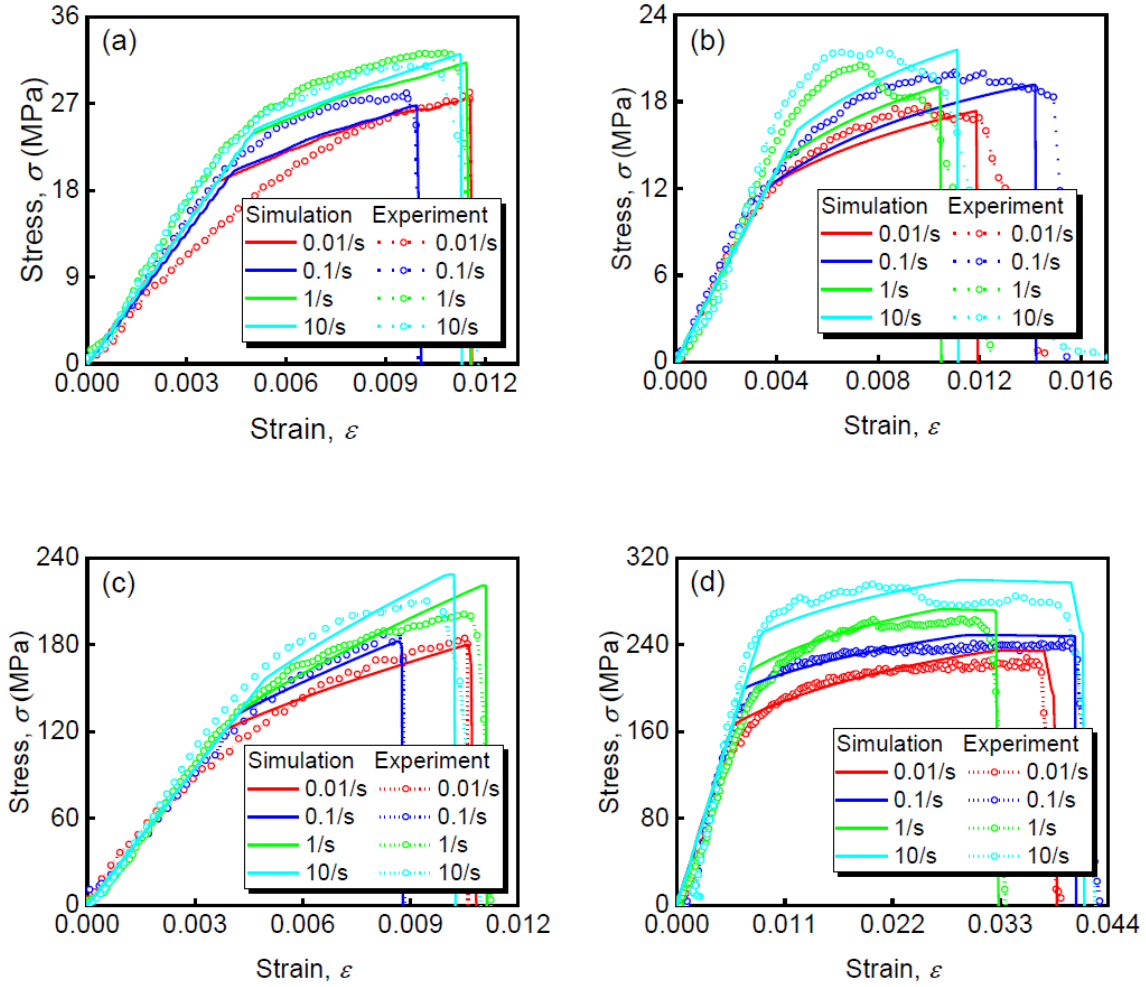

Fig.8. Stress vs strain comparison of experiment and simulation curves at 0.01/s, 0.1/s, 1/s, 10/s strain rates along 0° for: (a) cathode electrode with active material at SOC=0, (b) anode electrode with active material at SOC=0, (c) cathode current collector at SOC=0, (d) anode current collector at SOC=0.

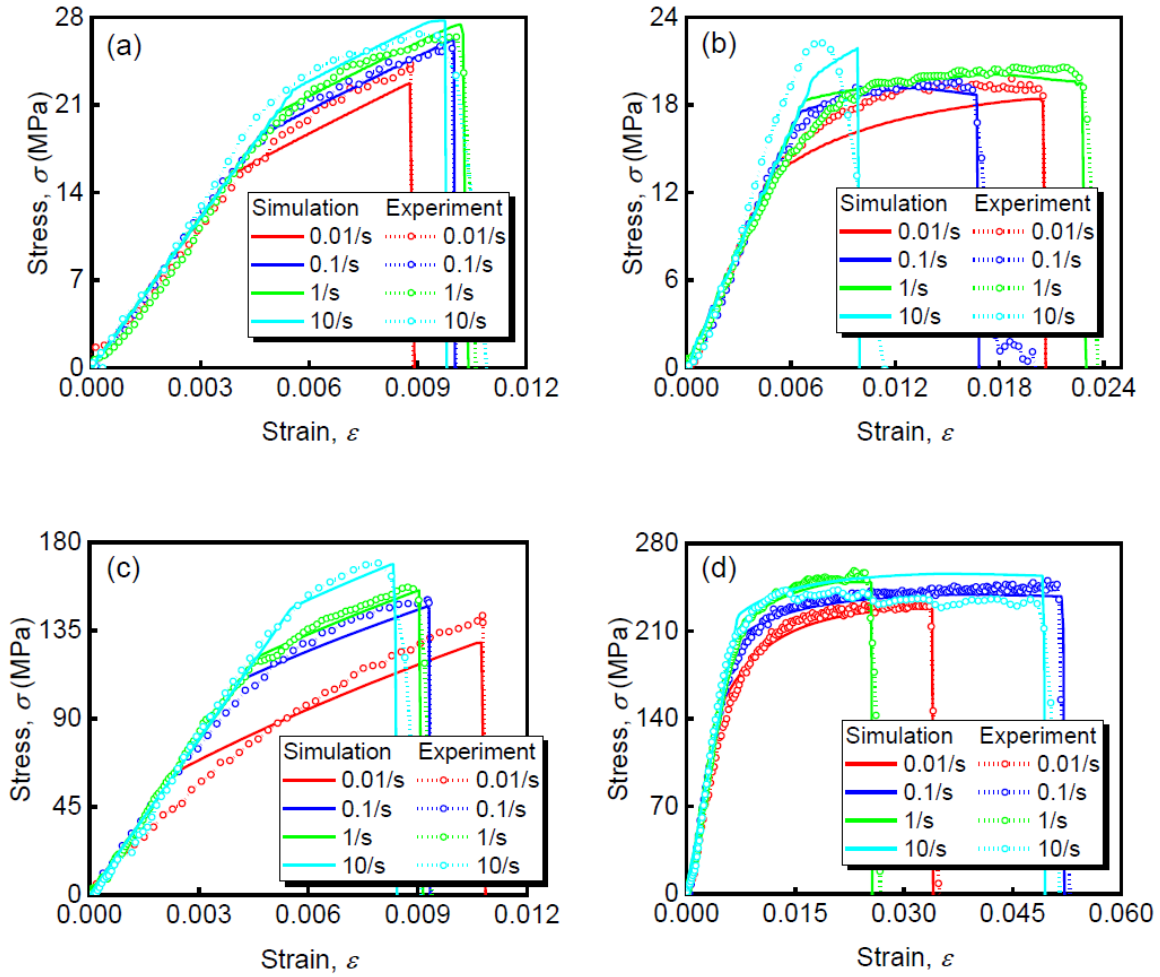

Fig.9. Stress vs strain comparison of experiment and simulation curves at 0.01/s, 0.1/s, 1/s, 10/s strain rates along 90° for: (a) cathode electrode with active material at SOC=0, (b) anode electrode with active material at SOC=0, (c) cathode current collector at SOC=0, (d) anode current collector at SOC=0.

4.2 Strain rate effect

As for Figs. 5, 8, and 9, it can be observed each of the cathode, anode, cathode current collector, and anode current collector samples for all three-angle orientation follow the strain rate effect. Table 2 provides the explanation for the claim of the strain rate effect as all the samples have a slightly high yield stress σ_y value for a higher strain rate. For example, the first sample cathode electrode with active material along 0° at SOC=0, σ_y = 18.77 MPa, 21.56 MPa, 23.78 MPa and 24.68 MPa for $\dot{\varepsilon} = 0.01$ s^{-1}, 0.1 s^{-1}, 1 s^{-1}, and 10 s^{-1}, respectively. The largest difference in the yield stress σ_y values between each strain rate is in the anode current

collector and cathode current collector samples. The yield strain ε_y for all those samples varies due to possible minor damage during the sample fabrication. Each of the material in electrode fabrication plays a vital role, which is deduced as from the strain rate effect. Since the anode and cathode overall shows isotropicity that is why these electrodes can be considered homogeneous. As the strain rate increases which increases the loading speed showing that the electrodes possess increased strength at higher strain rates under loading, similar to the current collector (i.e. aluminum and copper foils) without isotropicity. This indicates that active materials/particles of the electrodes have strong anisotropicity over the anode and cathode. The strain rate effect in the numerical simulation was governed by the Johnson-Cook model validated with the experiment performed. The agreement of simulation and experimental curves from Figs. 5, 8, and 9 provide the justification of the strain rate coupling phenomenon with mechanical behavior.

4.3 SOC effect

Figs. 10 (a)-(d) show that the comparison of anode electrode for 45° in all SOC scenarios. The comparison illustrates that the material becomes stiffer with the SOC, which is justified from the experimental work that, as the SOC increases the thickness of the anode electrode increases as well and since the stiffness is proportional to the cubic of the thickness, the material at higher SOC becomes stiffer. Failure strain ε_f gradually decreases with increasing SOC, indicating that the material becomes more brittle. Similar SOC comparison for the anode current collector, cathode electrode, and the pure current collector can be noticed in Figs. 10 (e)-(h), 11 (a)-(d) and (e)-(h), respectively. From these curves, it is discovered that the mechanical behaviors of anode current collector are independent of SOC. If we concentrate on the cathode and its current collector, we can see a reverse effect of the anode in SOC, i.e., as the SOC of the battery increases, the stress-strain curve drops. Hence, we see SOC=0 case

has the highest stress-strain curve, and SOC=0.6 has the lowest one. In terms of the failure strainε_f, it decreases with the strain rate, is a general phenomenon for both electrodes and current collectors. With increasing SOC there is volume expansion in the anode active material i.e., graphite. Graphite increases in volume up to 6.18 % from SOC = 0 to SOC = 0.6. This volume expansion is a result of the transfer of Li ions or lithiation. Li ions from cathode move to anode, allowing volume reduction. The change in thickness observed for the cathode is 5 μm, which results in the volume is reduced to 2.98 % from SOC = 0 to SOC = 0.6. Cathode being a denser material as compared to the graphite anode, it is observed there is no significant change in the thickness, yet volume change is notable [27]. Even though the thickness increases and hence the stiffness, the cathode electrode tends to be more brittle in nature and fail easily. With increasing SOC the current collector corrosion increases as the ion and electron transfer makes the electrode degrade with time which affects the performance of the battery. The corrosion in cathode current collectors is more significant than that in anode current collectors. Minor changes in the curves are noticed in the anode current collector, while a very significant change can be seen in the cathode current collector which can be seen from Figs. 10 and 11. The reason for this behavior is due to the binding of the active materials and current collectors. The binding of cathode active material and its current collector is stronger as compared to that of anode making cathode more vulnerable as deposition of Li ions over the current collector facilitates the corrosion. [28, 29]. For the cathode current collector, the thickness measured for all SOCs is 0.027±0.003 mm without any obvious SOC dependency . Therefore no change in stiffness is observed, yet the stress and strain curve drops as SOC increases. The charging and discharging of the battery results in Li-ion transfer leading the change in the concentration of Li-ions in each electrode may be one of the possible reasons for this behavior.

Table. 2. Material properties: Calculated yield stress σ_y and yield strain ε_y for different orientations and the materials at SOC=0.

Sample	Strain rate	0°		45°		90°	
		Yield stress, (σ_y) (MPa)	Yield strain, (ε_y)	Yield stress, (σ_y) (MPa)	Yield strain, (ε_y)	Yield stress, (σ_y) (MPa)	Yield strain, (ε_y)
Cathode with active material	0.01/s	18.77	0.00744	20.1622	0.00797	15.456	0.00506
	0.1/s	21.56	0.00476	22.2403	0.00921	18.599	0.00631
	1/s	23.78	0.00484	22.9385	0.00965	20.4284	0.00686
	10/s	24.681	0.00498	24.0393	0.00581	22.3522	0.00662
Anode with active material	0.01/s	11.107	0.00384	15.1654	0.00565	14.304	0.00563
	0.1/s	11.281	0.00324	16.139	0.00563	17.579	0.00973
	1/s	13.855	0.00362	17.501	0.00516	18.3974	0.01171
	10/s	15.988	0.00378	20.5227	0.0068	20.1023	0.00548
Cathode current collector	0.01/s	121.5037	0.00503	96.557	0.00457	62.535	0.00333
	0.1/s	132.46	0.00386	103.1357	0.00499	109.5349	0.00552
	1/s	135.4029	0.00281	113.2091	0.00568	121.8785	0.00538
	10/s	156.6249	0.00263	131.8764	0.00671	146.866	0.00513
Anode current collector	0.01/s	165.8093	0.00964	167.211	0.00661	151.7643	0.00638
	0.1/s	200.1748	0.01481	182.5578	0.00671	200.0828	0.01075
	1/s	216.2781	0.00972	180.9328	0.00547	206.314	0.00903
	10/s	251.629	0.01294	200.4761	0.0051	220.0688	0.01171

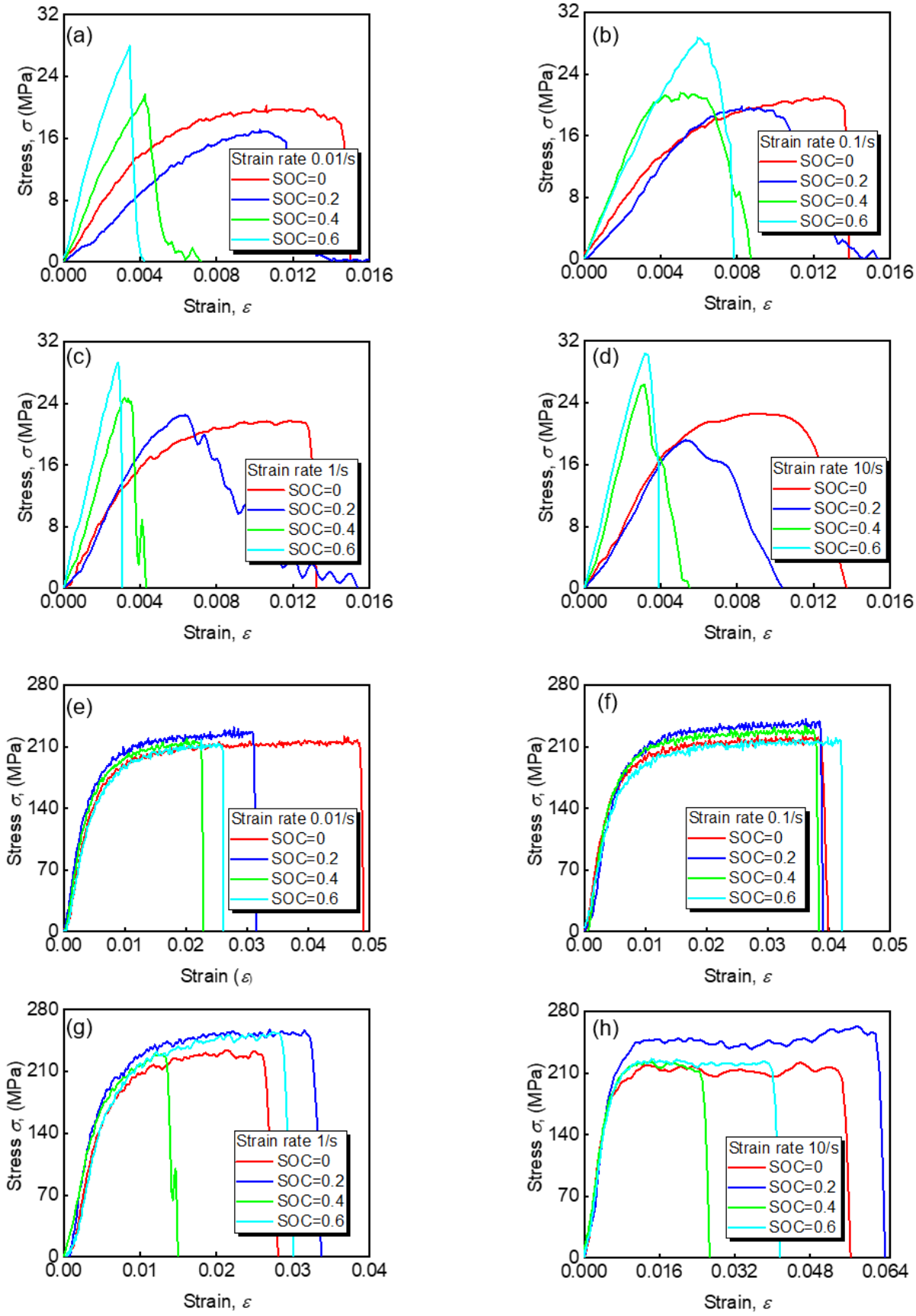

Fig.10. Stress vs strain curves for anode electrode with active material samples comparing different SOC (i.e. 0, 0.2, 0.4 and 0.6) along 45° for strain rate of: (a) 0.01/s, (b) 0.1/s, (c) 1/s, (d) 10/s, for

anode current collector samples comparing different SOC (i.e. 0, 0.2, 0.4 and 0.6) along 45° for strain rate of: (e) 0.01/s, (f) 0.1/s, (g) 1/s, (h) 10/s.

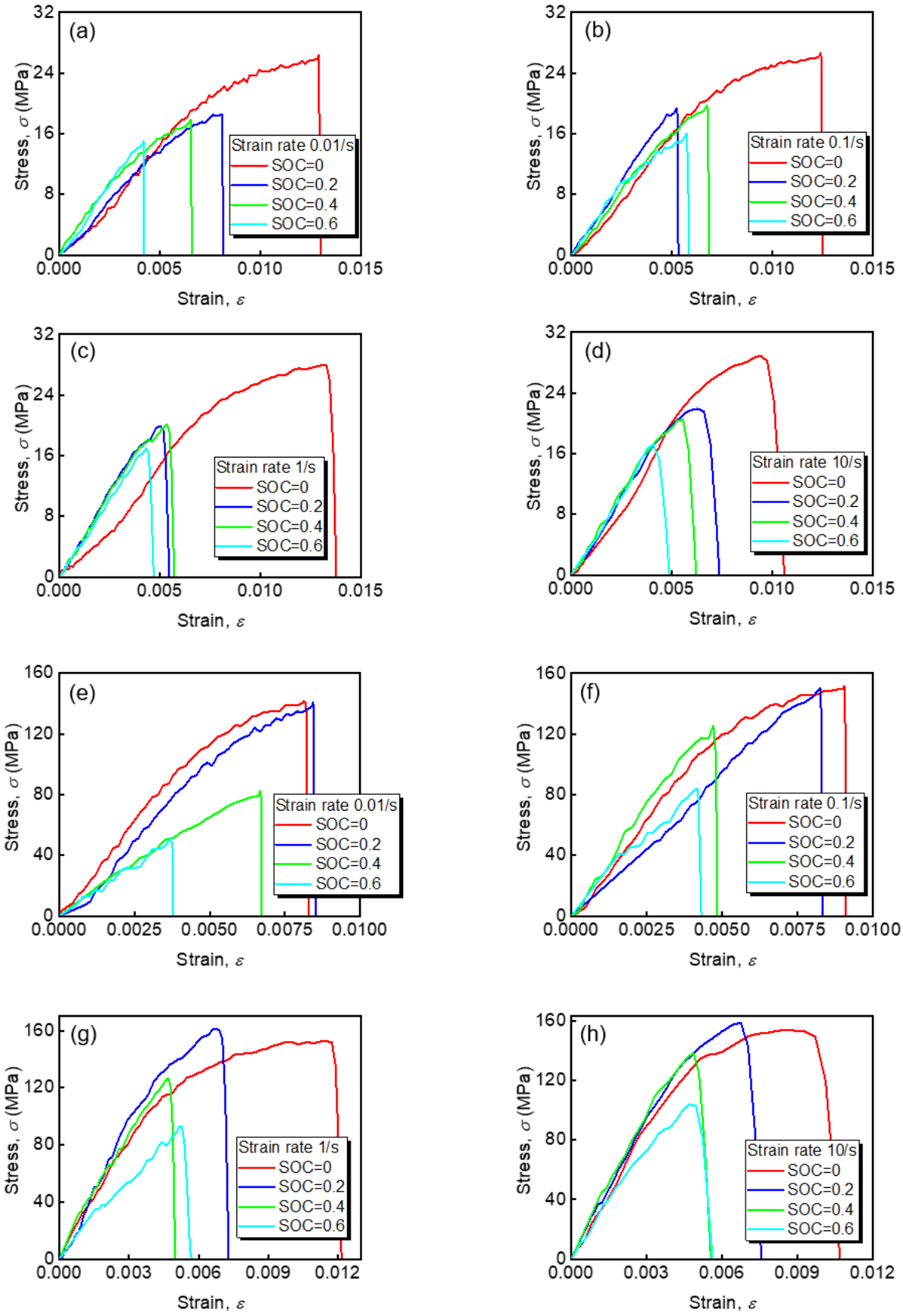

Fig.11. Stress vs strain curves for cathode electrode with active material samples comparing different

SOC (i.e. 0, 0.2, 0.4 and 0.6) along 45° for strain rate of: (a) 0.01/s, (b) 0.1/s, (c) 1/s, (d) 10/s, for cathode current collector samples comparing different SOC (i.e. 0, 0.2, 0.4 and 0.6) along 45° for strain rate of: (e) 0.01/s, (f) 0.1/s, (g) 1/s, (h) 10/s.

5. Conclusion

As a new widely used high-density cylindrical battery, the safety behavior of 21700 cells upon mechanical loading has become a heated topic. However, a pre-requisite understanding of it should be the mechanical behavior of the battery component materials upon various electrochemical statuses. In this study, the mechanical behavior of the anodes and cathodes in 21700 M50 LIB cells was investigated by tensile experiments. With the experiment validating simulation study conducted as understood for strain rates from 0.01 s^{-1}up to 10 s^{-1}, following conclusions were drawn and are listed as follows:

- With a variation in the orientation of the electrodes, the mechanical and electrochemical properties change, proving a strong anisotropic effect.
- Both electrodes and the current collectors have high strain-rate dependence at all angle orientations and even at different SOC of the battery.
- The SOC effect is dominating for anode, cathode, and cathode current collector, but not for anode current collector. The anode shows an obvious incremental trend of increasing stress with SOC, whereas surprisingly, the cathode and its current collector have a decremental trend.

Results provide a comprehensive characterization and understanding of the mechanical behaviors of electrodes in lithium-ion batteries and useful numerical models to guide the future safety design, evaluation, and monitoring of the batteries.

References

[1] B. Liu, Y. Jia, C. Yuan, L. Wang, X. Gao, S. Yin and J. Xu. Safety issues and mechanisms of lithium-ion battery cell upon mechanical abusive loading: A review, Energy Storage Materials 24 (2020) 85-112.
[2] B. Scrosati and J. Garche. Lithium batteries: Status, prospects and future, Journal of Power Sources 195 (2010) 2419-2430.
[3] J. B. Goodenough and Y. Kim. Challenges for Rechargeable Li Batteries†, Chemistry of Materials 22 (2010) 587-603.
[4] P. Peng and F. Jiang. Thermal safety of lithium-ion batteries with various cathode materials: A numerical study, International Journal of Heat and Mass Transfer 103 (2016) 1008-1016.
[5] L. Wang, S. Yin, C. Zhang, Y. Huan and J. Xu. Mechanical characterization and modeling for anodes and cathodes in lithium-ion batteries, Journal of Power Sources 392 (2018) 265-273.
[6] L. Wang, X. Duan, B. Liu, Q. M. Li, S. Yin and J. Xu. Deformation and failure behaviors of anode in lithium-ion batteries: Model and mechanism, Journal of Power Sources 448 (2020)
[7] W. Li, Y. Xia, J. Zhu and H. Luo. State-of-Charge Dependence of Mechanical Response of Lithium-Ion Batteries: A Result of Internal Stress, Journal of The Electrochemical Society 165 (2018) A1537-A1546.
[8] G. Kermani and E. Sahraei. Review: Characterization and Modeling of the Mechanical Properties of Lithium-Ion Batteries, Energies 10 (2017)
[9] A. Barré, B. Deguilhem, S. Grolleau, M. Gérard, F. Suard and D. Riu. A review on lithium-ion battery ageing mechanisms and estimations for automotive applications, Journal of Power Sources 241 (2013) 680-689.
[10] D. Shi, X. Xiao, X. Huang and H. Kia. Modeling stresses in the separator of a pouch lithium-ion cell, Journal of Power Sources 196 (2011) 8129-8139.
[11] P. Ping, Q. Wang, P. Huang, J. Sun and C. Chen. Thermal behaviour analysis of lithium-ion battery at elevated temperature using deconvolution method, Applied Energy 129 (2014) 261-273.
[12] B. Liu, Y. Jia, J. Li, S. Yin, C. Yuan, Z. Hu, L. Wang, Y. Li and J. Xu. Safety issues caused by internal short circuits in lithium-ion batteries, Journal of Materials Chemistry A 6 (2018) 21475-21484.
[13] C. Yuan, X. Gao, H. K. Wong, B. Feng and J. Xu. A Multiphysics Computational Framework for Cylindrical Battery Behavior upon Mechanical Loading Based on LS-DYNA, Journal of The Electrochemical Society 166 (2019) A1160-A1169.
[14] L. Wang, S. Yin and J. Xu. A detailed computational model for cylindrical lithium-ion batteries under mechanical loading: From cell deformation to short-circuit onset, Journal of Power Sources 413 (2019) 284-292.
[15] E. Sahraei, M. Kahn, J. Meier and T. Wierzbicki. Modelling of cracks developed in lithium-ion cells under mechanical loading, RSC Advances 5 (2015) 80369-80380.
[16] J. Xu, B. Liu, X. Wang and D. Hu. Computational model of 18650 lithium-ion battery with coupled strain rate and SOC dependencies, Applied Energy 172 (2016) 180-189.
[17] L. Greve and C. Fehrenbach. Mechanical testing and macro-mechanical finite element simulation of the deformation, fracture, and short circuit initiation of cylindrical Lithium ion battery cells, Journal of Power Sources 214 (2012) 377-385.
[18] Z. Pan, T. Sedlatschek and Y. Xia. Effect of State-of-Charge and Air Exposure on Tensile Mechanical Properties of Lithium-Ion Battery Electrodes, Journal of The Electrochemical Society 167 (2020)

[19] J. Xu, L. Wang, J. Guan and S. Yin. Coupled effect of strain rate and solvent on dynamic mechanical behaviors of separators in lithium ion batteries, Materials & Design 95 (2016) 319-328.
[20] J. Xu, B. Liu and D. Hu. State of Charge Dependent Mechanical Integrity Behavior of 18650 Lithium-ion Batteries, Sci Rep 6 (2016) 21829.
[21] S. Abada, G. Marlair, A. Lecocq, M. Petit, V. Sauvant-Moynot and F. Huet. Safety focused modeling of lithium-ion batteries: A review, Journal of Power Sources 306 (2016) 178-192.
[22] C. Yuan, L. Wang, S. Yin and J. Xu. Generalized separator failure criteria for internal short circuit of lithium-ion battery, Journal of Power Sources 467 (2020)
[23] W.-J. Lai, M. Y. Ali and J. Pan. Mechanical behavior of representative volume elements of lithium-ion battery modules under various loading conditions, Journal of Power Sources 248 (2014) 789-808.
[24] E. Sahraei, E. Bosco, B. Dixon and B. Lai. Microscale failure mechanisms leading to internal short circuit in Li-ion batteries under complex loading scenarios, Journal of Power Sources 319 (2016) 56-65.
[25] J. Zhu, J. Feng and Z. Guo. Mechanical properties of commercial copper current-collector foils, RSC Adv. 4 (2014) 57671-57678.
[26] S. Zhang, M. Sakane, T. Nagasawa and K. Kobayashi. Mechanical Properties of Copper Thin Films Used in Electronic Devices, Procedia Engineering 10 (2011) 1497-1502.
[27] X. Zhang, W. Shyy and A. Marie Sastry. Numerical Simulation of Intercalation-Induced Stress in Li-Ion Battery Electrode Particles, Journal of The Electrochemical Society 154 (2007)
[28] X. Zhang, P. N. Ross, R. Kostecki, F. Kong, S. Sloop, J. B. Kerr, K. Striebel, E. J. Cairns and F. McLarnon. Diagnostic Characterization of High Power Lithium-Ion Batteries for Use in Hybrid Electric Vehicles, Journal of The Electrochemical Society 148 (2001)
[29] E. Kramer, S. Passerini and M. Winter. Dependency of Aluminum Collector Corrosion in Lithium Ion Batteries on the Electrolyte Solvent, ECS Electrochemistry Letters 1 (2012) C9-C11.